Catalytically active membrane-like devices: ionic liquid-hybrid organosilicas decorated with palladium nanoparticles

Leandro Luza,[†] Camila P. Rambor,[†] Aitor Gual,[§] Fabiano Bernardi,[‡] Josiel B. Domingos,[χ] Thomas Grehl,[∫] Philipp Brüner[∫] and Jairton Dupont[†§*]

[†] Insitute of Chemistry, Universidade Federal do Rio Grande do Sul, Av. Bento Gonçalves 9500, Porto Alegre, Brazil.

[§] School of Chemistry, University of Nottingham, University Park, Nottingham, UK

[‡] Institute of Physics, Universidade Federal do Rio Grande do Sul, Av. Bento Gonçalves 9500, Porto Alegre, Brazil.

[χ] Departamento de Química – CFM, Campus Universitário Trindade, Universidade Federal de Santa Catarina, Florianópolis, Brazil.

[∫] ION-TOF GmbH, Heisenbergstr 15, 48149 Münster, Germany

Supporting Information Placeholder

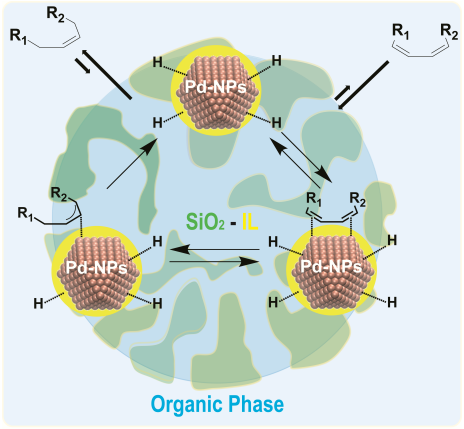

ABSTRACT: Ionic liquid (IL)-hybrid organosilicas based on 1-*n*-butyl-3-(3-trimethoxysilylpropyl)-imidazolium cations associated with hydrophilic and hydrophobic anions decorated with well dispersed and similar sized (1.8–2.1 nm) Pd nanoparticles (Pd-NPs) are amongst the most active and selective catalysts for the partial hydrogenation of conjugated dienes to monoenes. The location of the sputter-imprinted Pd-NPs on different supports, as determined by RBS and HS-LEIS analysis, is modulated by the strength of the contact ion pair formed between the imidazolium cation and the anion, rather than the IL-hybrid organosilica pore size and surface area. In contrast, the pore diameter and surface area of the hybrid supports display a direct correlation with the anion hydrophobicity. XPS analysis showed that the Pd(0) surface component decreases with increasing ionic bond strength between the imidazolium cation and the anions (contact ion pair). The finding is corroborated by changes in the coordination number associated with the Pd-Pd scattering in EXAFS measurements. Hence, the interaction of the IL with the metal surface is found to occur via IL contact pairs (or aggregates). The observed selectivities of ≥99% to monoenes at full diene conversion indicate that the selectivity is intrinsic to the electron deficient Pd-metallic surfaces in this "restricted" ionic environment. This suggests that IL-hybrid organosilica/Pd-NPs under multiphase conditions ("dynamic asymmetric mixture") operate akin to *catalytically active membranes*, *i.e.* far from the thermodynamic equilibrium. Detailed kinetic investigations show that the reaction rate is zero-order with respect to hydrogen and dependent on the fraction of catalyst surfaces covered by either the substrate and/or the product. The reaction proceeds via rapid inclusion and sorption of the diene to the IL/Pd metal surface saturated with H species. This is followed by reversible hydride migration to generate a π-allyl intermediate. The reductive elimination of this intermediate, the formal rate-determining step (RDS), generates the alkene that is rapidly expelled from the IL phase to the organic phase.

KEYWORDS: *SILP, sputtering-deposition, palladium, supported ionic liquid, hydrogenation.*

1. INTRODUCTION

It is well known that for many metal-catalyzed reactions the support influences the catalytic properties of the metal particles.[1] Indeed, the strong metal support interaction (SMSI) effect was reported several years ago.[2] The SMSI effect may be due to geometrical or electronic effects (charge transfer between support and nanoparticle).[3,4] For example, in the case of a geometrical effect, the metallic nanoparticles (M-NPs) are capped by functional groups from the support that migrate to the surface of the nanoparticles during the reaction.[5] Indeed, the capping layer can create new catalytically active sites or also block access to them, the latter being detrimental for the catalytic properties of the nanoparticles.[6] In this vein there are some reports on support effects in supported ionic liquid phase catalysts (SILP) resulting from the association of metal complexes or metal nanoparticles in ILs with various organic and inorganic supports.[7,8] However, the SMSI effect is still not perfectly understood, especially for the case where the IL is covalent bonded to the support. Therefore, shedding light into this important effect is crucial in order to project a new generation of more active and selective SILP catalysts. The IL support effect can be either geometrical and/or electronic but also as a physical barrier controlling the access or removal of reagents, intermediates and products from the catalytically active site.[9] This process looks like flowing liquid(s) (reagents and products) through a chemically active membrane[10] composed of SILP/NPs in confined space[11,12] (Scheme 1), *i.e.*, a non-equilibrium phenomenon. A principal point of this non-equilibrium is that all the chemical transformations as well as the other physico-chemical phenomena occurring with a catalyst in the course of its operation have to be considered as being inherently linked to the main "coupling" reaction.[13-16] Indeed, the formation of ionic cages around organometallic complexes in thin films of SILP has already been shown.[17]

Scheme 1. Schematic representation of immobilized catalysts in IL membrane-like device.

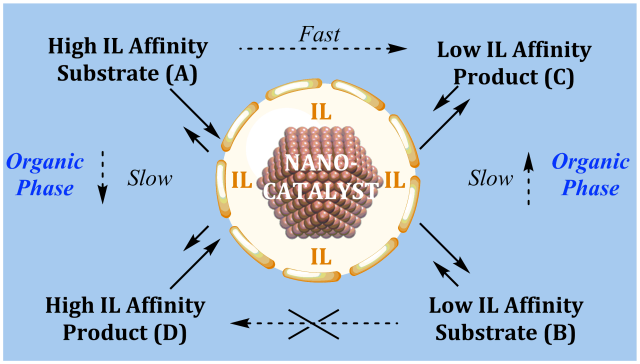

Very recently we reported a strong catalytic support effect in palladium nanoparticles (Pd-NPs) supported on IL-hybrid organosilicas. Apparently, the IL hydrophobicity plays a central role in the selective hydrogenation of dienes to monoenes by controlling the diene access to NP surface active sites.[18] However, the nature of the interaction between metal and the hybrid support is poorly understood. The main goal of this contribution is to understand the nature of the metal-support interaction and to relate the support-induced changes in catalytic properties to the changes in electronic properties of the M-NPs. For this work we have chosen hybrid organosilicas prepared by sol–gel processes using 1-*n*-butyl-3-(3-trimethoxysilylpropyl)-imidazolium cations associated with hydrophilic and hydrophobic anions which can be easily decorated with well dispersed and similar size (1.8–2.1 nm) Pd-NPs by simple sputtering-deposition. Moreover, these IL-hybrid materials display solid-membrane like properties [19] and their properties have been investigated in detail.[20-23]

The sputtering method is quite useful since the size of Pd-NPs can be easily controlled by the current discharge and metal concentration by the time of sputtering.[24-26] Moreover, in this method no by-products are generated and only Pd and the support are present in the catalytic material thus allowing a more accurate analysis of the interface Pd-support. Finally, the selective hydrogenation of 1,3-dienes was chosen as a probe to evaluate the properties of the catalysts since this reaction is structure sensitive. Indeed, their catalytic performance depends on M-NPs' size and shape.[27] Herein, we present in detail the depth-profile characterization of "naked" Pd-NPs - prepared by sputtering-deposition - by Rutherford Backscattering Spectrometry (RBS) and High Sensitivity-Low Energy Ion Scattering (HS-LEIS). Moreover, X-Ray Photoelectron Spectroscopy (XPS) and Extended X-ray Absorption Fine Structure (EXAFS) techniques investigated the interaction of the Pd-NPs with the support. Finally, the surface catalytic properties of the Pd-NPs were accessed through kinetics of the selective hydrogenation of 1,3-dienes to monoenes.

2. EXPERIMENTAL SECTION

2.1. General Procedures

All syntheses were performed using standard Schlenk techniques under argon atmosphere. Chemicals were purchased from Sigma-Aldrich and purified by standard procedures.[28] H_2 (> 99.999%) and D_2 (D > 99.8%) were purchased from White-Martins.

2.2. Catalyst Preparation and Characterization

The ILs based on 1-*n*-butyl-3-(trimethoxysilylpropyl)-imidazolium cation,[29] IL-hybrid organosilicas (**sg0**–**sgNTf$_2$**) and catalysts (Pd/**sg0**–Pd/**sgNTf$_2$**) were prepared according to procedures reported elsewhere.[18] Briefly, 1.0 g of the IL-hybrid organosilica (**sg0**–**sgNTf$_2$**) was placed in a conical Al flask inside a vacuum chamber. The chamber was closed and its pressure lowered to a base pressure of 4 µbar. The support was then evacuated for 4 h, after which the vacuum chamber was placed under a sputtering working pressure of 4 mbar by adding Ar flow. The support was continuously homogenized by revolving the Al flask at a frequency of 24 Hz. Pd was sputtered onto the revolving support at a 35 mA discharge current for 3.0 min. After the deposition, the chamber was vented with N_2 and the grey powder was recovered and stored under Ar for their further characterization and application. Details of the chamber containing an electro-magnetic oscillator with variable controlled frequency, which allows the constant movement of the conical flask, are described elsewhere.[30,31]

Elemental analysis of the ILs immobilized on the support surfaces was carried out on a CHN Perkin Elmer M CHNS/O Analyzer, model 2400. N_2 isotherms of the catalysts, previously degassed at 100 °C under vacuum for 3 h, were obtained using Tristar 3020 Micromeritics equipment. Specific surface areas were determined by the BET multipoint method and average pore size was obtained by BJH method. Pd content was determined by X-ray fluorescence (XRF) carried out using a Shimadzu XRF-1800 sequential X-ray fluorescence

spectrometer. Samples were prepared in KBr and calibration was performed using bromine as an internal standard. STEM samples were prepared by the slow evaporation of a drop of each colloidal solution of isopropanol deposited under an argon atmosphere onto a holey carbon-covered copper grid. STEM measurements were performed with a XFEG Cs-corrected FEI Titan 80/300 electron microscope operating at 200 kV at INMETRO/RJ. Rutherford backscattering spectroscopy (RBS) measurements were carried out in a 3 MV Tandetron accelerator using a He^+ ion beam of 1.5 MeV at IF/UFRGS. The Si surface-barrier detector was positioned at a scattering angle of 165°. High sensitivity-low energy ion scattering (HS-LEIS) measurements were performed using the advanced analyzer Qtac100 (ION-TOF GmbH, Germany) in the static depth-profiling mode. A 3 keV $^4He^+$ ion beam was focused in the sample with normal incidence and the scattered ions were detected at an angle of 145°. The analyzed area was 2 x 2 mm^2. The sputtered ions were separated from the $^4He^+$ scattered ions by using a pulsed ion beam and time-of-flight filtering procedure. A Pd reference foil was measured after cleaning the surface by means of ion sputtering for comparison purposes.

X-ray photoelectron spectroscopy (XPS) measurements were carried out at the LNLS (Brazilian Synchroton Light Laboratory) at the SXS beam line endstation.[32] The spectra were collected using an InSb (111) double crystal monochromator at fixed photon energy of 1,840 eV. The sample was investigated using the long scan, Pd 3d, O 1s and C 1s scan regions. This photon energy gives an inelastic mean free path for the photoelectrons coming from the Pd 3d electronic level of $\lambda \approx 4$ nm. The hemispherical electron analyzer (PHOIBOS HSA500 150 R6) was set at a pass energy of 30 eV and the energy step was 0.1 eV, with an acquisition time of 100 ms/point. The overall resolution was around 0.3 eV. The base pressure inside the chamber was around 5 x 10^{-9} mbar. The monochromator photon energy calibration was done at the Si K edge (1,839 eV). An additional calibration of the analyzer energy was performed using a standard Au foil (Au $4f_{7/2}$ peak at 84.0 eV). The XPS measurements were obtained at a 45° take off angle at room temperature. XPS Peak version 4.1 was used to fit the XPS results. All peaks were adjusted using a Shirley type background and an asymmetric Gaussian-Lorentzian sum function (27% Lorentzian contribution), as determined from the XPS measurement at the Au 4f region of the standard Au foil. The fitting at the Pd 3d electronic level was performed considering the well-known satellite peaks due to the shake-up effect associated to Pd.[33] X-ray Absorption Spectroscopy (XAS) measurements were performed in transmission mode at the LNLS at the XDS beamline endstation using about 1.0 g of the Pd/SiO_2 powder inserted into a cuvette. The spectra were collected at the Pd K edge (24,350 eV) using a Si (311) monochromator and three ionization chambers filled with Ar gas. A standard Pd foil was used to calibrate the monochromator. The spectra were acquired in the range of 24,250-24,900 eV with 0.5 eV (XANES region) and 2.0 eV (EXAFS region) steps and 2 s per point. Five to ten scans were acquired in order to improve the signal-to-noise ratio. All XAS spectra were recorded at room temperature. The EXAFS regions of the XAS data were analyzed in accordance with the standard procedure of data reduction[34] using IFEFFIT.[35] FEFF was used to obtain the phase shift and amplitudes.[36] The EXAFS signal $\chi(k)$ was extracted then Fourier-transformed using a Kaiser-Bessel window with Δk range of 7.0 $Å^{-1}$. All the data were k^2 weighted. Single scattering events were considered in the fitting procedure of the coordination shell. Based on the chemical components found in the XPS measurements, the FT fitting of the XAS measurements was performed including also a Pd−X scattering path, where X = Cl, F, N or O, depending on the sample studied. In the case of the Pd/**sg0** sample, a Pd−Si scattering due to the Si atoms from the SiO_2 support was included too in order to adjust the data. The Pd−Cl, Pd−F and Pd−N scattering comes from the interaction between the Pd nanoparticles and the anion used. The S_0^2 value was fixed at 0.79 as obtained from the adjustment of the Pd standard. The R-factor obtained from the analysis was always lower than 0.01, which demonstrates the excellent agreement between the proposed model and the experimental result.

2.3. Hydrogenation Performance

As a general procedure, 10 mL of a solution of the corresponding 1,3-diene (diene/Pd = 5000) dissolved in CH_2Cl_2 was added to a Fischer-Porter reactor containing the appropriate amount of catalyst (0.1 μmol Pd). After that, the reactor was pressurized with 4 bar of H_2 at 40 °C. Samples were taken from the reaction mixture and the conversion and selectivity were determined by GC-analysis of the reaction samples. After the desired reaction time, the reactor was cooled to room temperature and then depressurized. GC analyses were run with an Agilent Technologies GC System 6820: injector and detector (FID) temperature of 260 °C; N_2 as carrier (1 mL min^{-1}); column head pressure of 10 psi; temperature program from 40 °C (10 min) to 250 °C at a heating rate of 10 °C min^{-1}; DB-17 column (30 m × 0.25 mm × 0.25 μm) for the hydrogenation of 1,3-cyclohexadiene (**1**), cyclohexene (**2**), 1,4-cyclohexadiene (**5**), 1,3-cyclooctadiene (**6**), cyclooctene (**7**), 1,5-cyclooctadiene (**10**) and styrene (**11**); Alumina column (30 m × 0.43 mm) for the hydrogenation of 1,3-butadiene (**13**), 2-methyl-1,3-butadiene (**18**) and 2,3-dimethyl-1,3-butadiene (**23**); and HP-5 column (30 m × 0.20 mm × 0.30 μm) for the hydrogenation of *α*-terpinene (**27**).

2.4. Mechanistic and Kinetic Studies

For the deuterolabelling studies, a solution of the 1,3-cyclohexadiene (diene/Pd = 5000) in CH_2Cl_2 (10 mL) was added to a Fischer-Porter reactor containing the appropriate amount of catalyst (0.1 μmol Pd). After that, the reactor was pressurized with 4 bar of H_2 or D_2 at 40 °C. Samples were taken from the reaction mixture and the conversion and selectivity were determined by GC, GC-MS and ^1H, ^2H and ^{13}C NMR analysis of the reaction samples. After the desired reaction time, the reactor was cooled to room temperature and then depressurized. GC-MS analyses were run with a Shimadzu QP50 using a Rtx-5MS column (30 m × 0.25 mm × 0.10 μm); injector temperature of 260 °C; He as carrier (1 mL min^{-1}); the temperature program was from 40 °C (10 min) to 250 °C (10 min) at a heating rate of 10 °C min^{-1} and ionizing voltage of 70 eV. ^1H, ^2H and ^{13}C NMR analysis of the samples obtained by D_2 reduction of 1,3-cyclohexadiene (**1**) by Pd/**sg0** and Pd/**sgNTf$_2$** were performed by using a Varian 400 MHz spectrometer at the CNANO/UFRGS. The incorporation of D in the reaction products was quantified by comparing the ^1H NMR spectra with these obtained from a standard sample (relaxation delay = 1–10 s) and by performing ^2H NMR experiments (relaxation delay 10 s).

For the kinetic studies, solutions of the 1,3-cyclooctadiene (**6**) in CH_2Cl_2 (10 mL) of distinct concentrations (0.0125, 0.025, 0.05, 0.1 or 0.2 mol L^{-1}) were added to a Fischer-Porter reac-

tor containing the appropriate amount of catalyst (0.1 μmol Pd). After that, the reactor was pressurized with H_2 (2, 3, 4, 5, 6 or 8 bar) and heated (20, 40, 60, 80 or 100 °C). Samples were taken from the reaction mixture and the conversion and selectivity were determined by GC analysis of the reaction samples. GC analyses were run with an Agilent Technologies GC System 6820: injector and detector (FID) temperature of 260 °C; N_2 as carrier (1 mL min^{-1}); column head pressure of 10 psi; temperature program from 40 °C (10 min) to 250 °C at a heating rate of 10 °C min^{-1} with a DB-17 column (30 m × 0.25 mm × 0.25 μm). After the desired reaction time, the reactor was cooled to room temperature and then depressurized. Reaction rate was normalized to the total surface area of the nanoparticles per unit of volume. Kinetic and equilibrium constants were determined by mathematical non-linear fitting procedures at 20% conversion of the substrate.

3. RESULTS AND DISCUSSION

3.1. Metal Content and Depth-Profile Characterization

The catalytic materials based on IL-hybrid organosilicas were prepared by sputtering-deposition, yielding well-dispersed Pd-NPs with small mean diameters (Scheme 2, Table 1, Table S1 and Figures S1-S3).[18] There is no significant variation of the specific surface area, pore volume and diameter values after the metallic deposition. The Pd amount on the catalysts (Pd/**sg0**, Pd/**sgCl**, Pd/**sgNO$_3$**, Pd/**sgPF$_6$** and Pd/**sgNTf$_2$**) was determined by XRF analysis giving the following Pd contents: 0.125 *wt*%, 0.124 *wt*%, 0.122 *wt*%, 0.127 *wt*%, and 0.123 *wt*%, respectively (Table S1).[18]

Scheme 2. Synthesis of the IL-hybrid organosilicas decorated with palladium nanoparticles by sputtering-deposition.

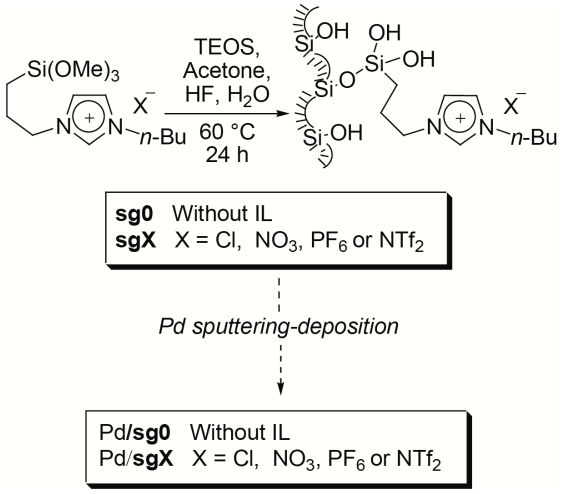

The pore diameter and surface area of the hybrid materials are directly related to hydrophobicity of the anion (Table 1), *i.e.*, highly water soluble ILs (containing Cl^- and NO_3^- anions) yield materials with higher surface areas and pore diameters than those associated with hydrophobic anions (PF_6^- and NTf_2^-). The reduction of the surface area in IL-hybrid organosilicas is usually produced by the filling of the small pores with IL.[37,38] In our case the relative reduction of the surface are as compared to Sg0 support is associated with the distinct size and distributions of pores produced by the IL templates containing different anions.

Depth-profile characterization of the catalysts was carried out by two distinct techniques, Rutherford backscattering spectroscopy (RBS) measurements and high sensitivity-low energy ion scattering (HS-LEIS) (Figure S4). A direct comparison between the metal percentage in the surface region by LEIS (down to around 10 nm) and RBS (20, 50 and 100 nm) is displayed in Figure 1.

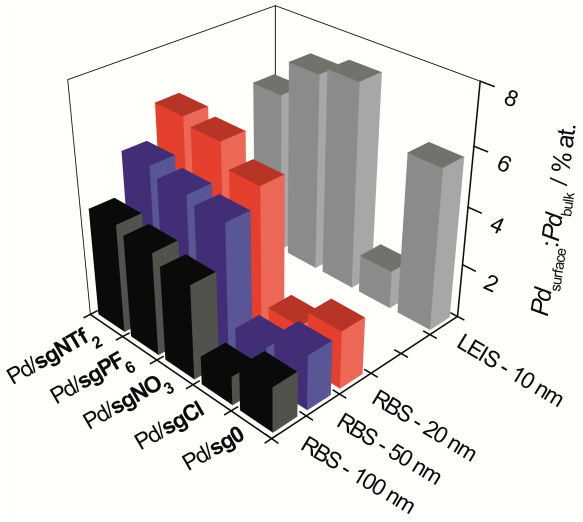

Figure 1. Percentage of Pd atoms close to the surface region of the Pd/**sg0**–Pd/**sgNTf$_2$** catalysts estimated by RBS and HS-LEIS techniques.

Table 1. Summary of the physical and chemical characteristics of the Pd/**sg0**–Pd/**sgNTf$_2$** catalysts.

Entry	Catalyst	S_{BET}/ m^2 g^{-1}[a]	Pore Diameter/ nm[a]	$d_{Pd\text{-}NPs}$/ nm[b]	Pd^0:$Pd^{\delta+}$/ %[c]
1	Pd/**sg0**	462	11.4	1.8	3/97
2	Pd/**sgCl**	375	6.6	1.8	1/99
3	Pd/**sgNO$_3$**	449	6.0	1.8	58/42
4	Pd/**sgPF$_6$**	287	3.4	2.1	41/59
5	Pd/**sgNTf$_2$**	276	3.0	1.8	36/64

[a] Determined by N_2 physisorption analysis; [b] Determined by STEM analysis; [c] Determined by XPS analysis.

The amount of metal of a given sample quantified by RBS is smaller than that quantified by LEIS measurements. It shows the depth profile is narrow and most of the Pd atoms are close to the surface region. Pd-NPs revealed no direct relationship with physical properties (pore diameter and surface area) of the supports obtained using anions with distinct polarities (hydrophobic *vs*. hydrophilic). Indeed, the depth-profile of Pd in the Pd/**sgPF$_6$** and Pd/**sgNTf$_2$** catalysts (containing hydrophobic anions, *i.e.*, small surface areas and pore diameters) is similar to the Pd/**sgNO$_3$** catalyst (hydrophilic anion, large surface area and pore diameter). Thus, the observed depth-profile has been attributed to the influence of the cation-anion interaction strength (in contact ion pairs).[39] In fact, the strength of cation-anion interaction increases in the order Im.NTf_2 ≈ Im.PF_6 < Im.NO_3 << Im.Cl correlating with the Pd depth-profile in the catalyst. Hence, catalytic materials in which the cation-anion interaction is weak Pd/**sgPF$_6$**, Pd/**sgNTf$_2$** and

Pd/**sgNO$_3$** (weakly coordinating anions) have a considerably higher Pd concentration at the outer surface with narrower Pd depth-profiles when compared to the catalyst with stronger cation-anion interactions (covalent-like interactions), Pd/**sgCl** (Figure 1).[40,41] Therefore, the location of the Pd-NPs on supports can be modulated by the strength of the contact ion pair formed between the imidazolium cation and the anion of the IL-hybrid organosilica. Higher internal Pd-NPs concentrations in the supports are formed in those containing strong contact ion pairs, i.e., less interaction of the IL ion pair (anion and cation) with the metal sputtered reactive species and thus favouring the diffusion of these species to internal layers. In summary after being sputtered from the target, the Pd atoms can stay at the hybrid support surface or preferentially diffuse deeper into the support. Therefore the stages of nucleation, growth of compact atomic clusters, aggregation of branched islands to form the NPs can occur preferentially at the metal surface or deeper inside the support depending on the strength of ion pairing between the IL cation and anion. Note that previously a pore-size dependency explanation was given by other authors in the synthesis of Ru-NPs sputtered on H-beta zeolites.[42]

It is also clear that the size and shape of NPs depends mainly on the sputtering conditions as already established earlier for the preparation of metal NPs and both liquid and solid supports, i.e., under the same sputtering conditions NPs with similar sizes and shapes are formed.[31,43-45] However, in the case of neat ILs there is also a strong influence of the type of the anion on the size and shape of the NPs.[44] Hence it is probable that the IL thin layer like properties are determined by the competition between the liquid/solid attraction, akin to that observed in physical mixtures of IL/silicon materials in which IL/solid attraction dominates when the film is thin.[46]

3.2. Chemical State and local atomic order of the Pd atoms

XAS was used to probe the local atomic order around the Pd atoms of the Pd/**sg0**–Pd/**sgNTf$_2$** catalysts (Figure 2). A strong dumping on the EXAFS oscillations and a variation of the FT amplitude of the peak associated with the Pd−Pd scattering when comparing signals of nanoparticles and standard is observed. This behavior was related to the low size of the Pd-NPs, since metal nanoparticles usually display lower coordination numbers associated to the metal−metal scattering, $N_{met-met}$, (Table S2).

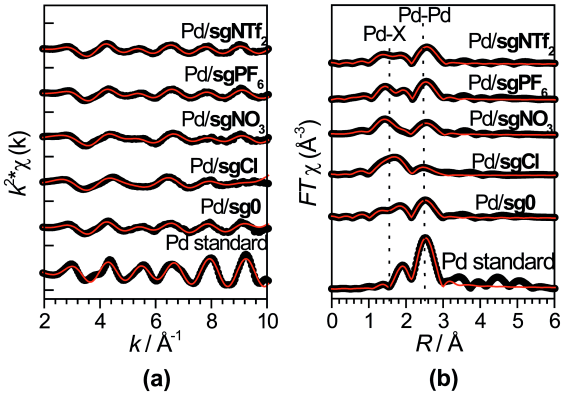

Figure 2. Comparison of the (a) EXAFS signals and (b) the corresponding Fourier transforms (FT) of the Pd/**sg0**–Pd/**sgNTf$_2$** catalysts (black points and red lines represent the experimental data and the best fit found, respectively).

It is possible to observe also a longer Pd-Pd distance in the nanoparticles if compared to bulk Pd (Table S2*)*. In fact, contraction of the metal-metal distance is typically observed as the particle size decreases.[47,48] However, in the case of Pd the opposite behavior (elongation of the Pd-Pd distance) is usually observed for Pd nanoparticles and it can be attributed to a structural change,[49], pseudomorphism[50] or incorporation of a foreign atom (like H, C, O) in the lattice.[51]

Among the Pd-NPs, the high cation-anion strength systems (*i.e.*, Pd/**sgC**l) resulted in higher N_{Pd-Pd} value and lower N_{Pd-X} value, whereas low cation-anion strength (*i.e.*, Pd/**SgNTf$_2$**) resulted in higher N_{Pd-Pd} value and lower N_{Pd-X} valueXPS was also employed to probe the chemical surface state of the Pd-NPs (Figure 3). Pd-NPs surfaces with no IL (Pd/**sg0**) or bearing the IL with the high ionic strength (Pd/**sgCl**) are quantitatively oxidized (ratio of Pd^0:$Pd^{\delta+}$ 3:97 and 1:99, respectively, Table 1). Whilst, Pd-NPs surfaces with the IL with low ionic strength (Pd/**NO$_3$**, Pd/**sgPF$_6$** and Pd/**sgNTf$_2$**) displayed more pronounced metallic character (58:42, 41:59 and 36:64, respectively, Table 1). The typical error on the Pd^0:$Pd^{\delta+}$ ratio is around 15% of the corresponding value. The binding energy position of Pd $3d_{5/2}$ electronic level corresponding to the Pd^0 component is expected to be at 334.9 eV for bulk Pd.[52] In this work, the binding energy position for Pd^0 components at Pd nanoparticles is found at around 335.2 eV, a value 0.3 eV higher than that associated to bulk Pd. This difference may be associated to the electron deficient character of the active Pd sites at the Pd nanoparticles. On the other hand, it is important to stress here that it is well known from the literature that the Pd 3d electronic level binding energy is dependent on the size of the Pd nanoparticles.[53] As the diameter of the Pd nanoparticles decreases the binding energy of a given component shifts to higher values. Since the mean diameter of the nanoparticles in this work is around 1.8 nm, the Pd components should be shifted to higher energies. Thus, both shifting effects are actually expected to occur in this case.

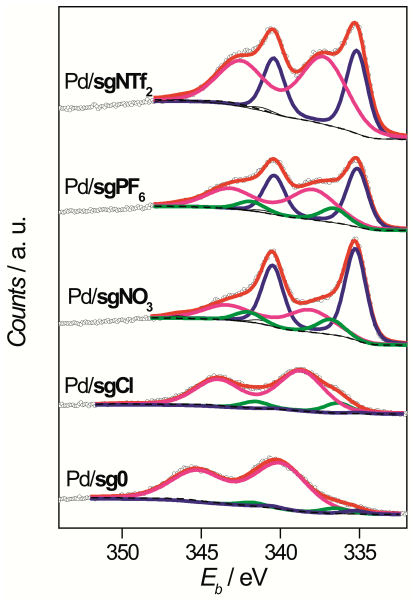

Figure 3. Pd 3d XPS spectra of the Pd/**sg0**–Pd/**sgNTf$_2$** catalysts (black points represent the experimental points, dash black line the Shirley background used, red solid line the fitting performed and the blue, green and magenta solid lines represent the Pd^0, Pd–O and Pd–X (X = Cl, N, F or O_2) components).

The component of higher binding energy found in the Pd/**sg0** catalyst is consistent with the PdO_2 component. The shift of this

component to lower binding energies in the other cases (Pd/**sgCl**, Pd/**sgNO$_3$** and Pd/**sgPF$_6$**/Pd/**sgNTf$_2$**) was attributed to the interaction of the Pd surface atoms with the IL atoms (*i.e.*, Cl, N and F), and thus the formation of an IL (mono)layer partially protected the Pd atoms against oxidation (Table S3). Therefore, the oxidized palladium component increases with the decrease of the ionic bond strength between the imidazolium cation and anions, *i.e.*, the stronger the ionic interaction between the cation and anion, the less "ionic" is the contact ion pair. Hence, the interaction of the IL with the metal surface is *via* IL contact pairs (or aggregates)[54,55] rather than by charged species, corroborating the proposed supramolecular model for formation and stabilization of M-NPs in ILs.[56-58]

3.3. Highly Active and Selective Hydrogenation Catalyst

Catalytic hydrogenation of several substrates was performed under previously optimized reaction conditions[18] using Pd/**sgPF$_6$** as the most active and selective catalyst (Table 2, Table S4 and Figure S5). It is observed that the cyclic conjugated dienes 1,3-cyclohexadiene (**1**), 1,3-cyclooctadiene (**6**) and styrene (**11**) differ from the isolated 1,4-cyclohexadiene (**5**) and 1,5-cyclooctadiene (**10**) since they are completely converted with higher activities when compared to the non-conjugated, albeit the heat of hydrogenation of conjugated and non-conjugated dienes is usually less than 4 kcal mol^{-1} (Table 2, Entries 1-5). This fact suggests that the hydrogenation of the dienes (structure sensitive reaction) by the Pd catalysts is also probably related to their affinity for the catalytically active sites.[59] Finally, non-conjugated dienes display similar reactivities of simple monoenes cyclohexene (**2**) and cyclooctene (**7**) (Table 2, Entries 2,4,10 and 11).

As expected, substituent groups affect the catalytic performance of the catalyst. Among the linear conjugated dienes the primary 1,3-butadiene (**13**) show higher activities than the secondary 2-methyl-1,3-butadiene (**18**), which in turn, was more reactive than the tertiary 2,3-dimethyl-1,3-butadiene (**23**). Moreover, the selectivity for the respective internal monoenes (**15**, **16**, **21** and **25**) increases in this same order, *i.e.*, by the consecutive introduction of methyl groups to the substrates (Table 2, Entries 6-8). The same reactivity trend was also observed in the hydrogenation of di-, tri- and tetra-substituted olefins by either Ir-NPs or classical homogenous catalysts supported in neat ILs.[60,61]

Table 2. Selective hydrogenation of dienes and α,β–unsaturated carbonyl compounds by Pd/**sgPF$_6$** catalyst under optimized reaction conditions.

E.[a,b]	Diene	TOF (Conv.)[c]	Products (Selectivity/ %)
1	 **1**	3.0 (>99)	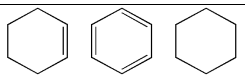 **2** (97) **3** (2) **4** (1)
2	 **5**	0.1 (<2)	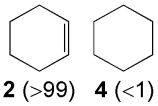 **2** (>99) **4** (<1)
3	 **6**	13.0 (>99)	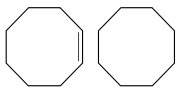 **7** (>99) **8** (<1)
4	 **10**	0.3 (<4)	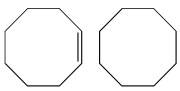 **7** (>99) **8** (<1)
5	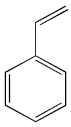 **11**	5.0 (85)	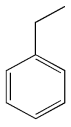 **12** (>99)
6	 **13**	11.6 (>99)	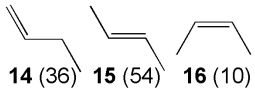 **14** (36) **15** (54) **16** (10)
7	 **18**	3.7 (>99)	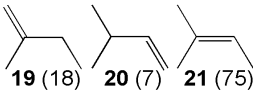 **19** (18) **20** (7) **21** (75)
8	 **23**	0.7 (>99)	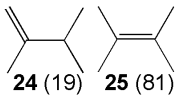 **24** (19) **25** (81)
9	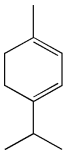 **27**	6.2 (>99)	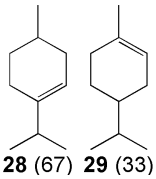 **28** (67) **29** (33)
10	 **2**	— (<1)	—
11	 **7**	— (<1)	—
12[d]	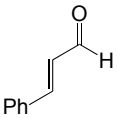 **30**	1.1 (>99)	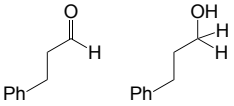 **31** (98) **32** (2)
13[d]	 **33**	3.7 (>99)	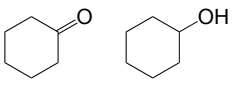 **34** (>99) **35** (<1)
14[d]	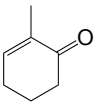 **36**	0.1 (>99)	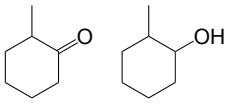 **37** (>99) **38** (<1)

[a] Reaction conditions: Pd/**sgPF$_6$** catalyst (0.1 μmol Pd), substrate/Pd = 5000, 10 mL of CH_2Cl_2, 4 bar H_2, 40 ºC and 250 rpm; [b] Conversion and selectivity determined by GC analysis; [c] TOF = mol substrate converted/(mol Pd surface × second) calculated from the slope of plots of TON *vs*. time at low substrate conversions and conversions calculated according to ref.[62]; [d] Reaction conditions: Pd/**sgPF$_6$** catalyst (0.1 μmol Pd), substrate/Pd = 5000, 5 mL of m-xylene, 4 bar H_2, 100 ºC and 250 rpm.

Interestingly, solely products obtained by 1,2-additon of hydrogen are observed in the selective hydrogenation of *α*-terpinene (**27**) with higher selectivity for the monoene in which the addition of hydrogen is at the less sterically hindered double bond (Table 2, Entry 9). Unlike in the hydrogenation of the 1,3-cyclohexadiene (**1**), no disproportionation of the substrate was observed. This fact can be associated to the presence of the substituent groups (methyl and isopropyl) that restrict the diene arrangement in the correct geometry for the transfer of hydrogen from one diene to another.

It is noteworthy that the high selectivity obtained for the monoenes (usually ≥99%) suggests that the selectivity is intrinsic to the Pd-metallic surfaces in this IL-hybrid organosilica environment, and probably, it is due to its highly electron deficient nature (Table 1) that displays higher adsorption affinity for the diene than to the monoene.[63-65] This suggests that SILP/Pd-NPs under multiphase conditions (dynamic asymmetric mixture)[66] operates akin to *catalytically active membranes*[67], *i.e.*, far from thermodynamic equilibrium.[68] In this case, the dienes, which are at least four times more soluble in the hybrid catalytic materials than the monoenes[69,70], displace the formed monoenes from the Pd-NP surface, which are then extracted by the organic phase (before reaching thermodynamic equilibrium). This catalytic system was also demonstrated to be effective in the hydrogenation of α,β–unsaturated aldehyde (**30**) and ketones (**33** and **36**) (Table 2, Entries 12-14).

Therefore, the selectivity of the Pd-NPs is not entirely related to the stronger Pd−H bonds on model Pd(100) than other metals as suggested earlier.[64] Pd-NPs embedded in ILs also achieved similar selectivities than those reported herein. Moreover, the selectivity for monoenes, during the hydrogenation of 1,3-butadiene (**13**) by the classical heterogeneous catalyst Pd/C (5% Degussa) in the presence of IL, is very low even at low substrate concentrations.[69]

3.5. Mechanistic and Kinetic Evidence of Palladium Surface Modification by IL (Mono)Layers

In order to clarify the influence of the IL (mono)layers over the reaction pathways of the hydrogenation/disproportionation of 1,3-cyclohexadiene (**1**), mechanistic studies under deuterium using the Pd/**sg0** and Pd/**NTf$_2$** catalysts were compared (Scheme 3).

Scheme 3. Deuterolabeling experiments to study the kinetic isotopic effect and the mechanism of the hydrogen addition (1,2- *vs*. 1,4-addition).

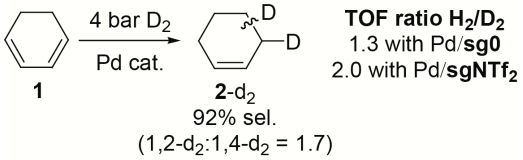

The Pd/**sg0** catalyst (H_2:D_2 TOF ratio = 1.3) and Pd/**sgNTf$_2$** catalyst (H_2:D_2 TOF ratio = 2.0) display a relatively small kinetic isotopic effect (Table S5 and Figure S6), typical of the secondary isotopic effect. Therefore, the H−H/D−D activation is probably not directly involved in the rate-determining step (RDS) (see below). Quantification of the reaction products (Figures S7-S9) allowed calculating the selectivity of **2**-d_2 as 92% with a 1,2:1,4 addition ratio of 1.7 which indicates that the reduction of the 1,3-cyclohexadiene (**1**) involves the formation of meta-stable π-allyl intermediates. This is in line with the assumption that the reaction occurs via reversible hydrogenation to a half-hydrogenated intermediate.[64] The formation of benzene (**3**) with no incorporation of D in its ring indicates the occurrence of disproportionation of the 1,3-cyclohexadiene (**1**) by a concerted step in which one H atom is transferred from one diene to another by an outer-sphere-like mechanism. Similar behavior was observed in hydrogenation reactions catalyzed by Pd/Al_2O_3 obtained by sputtering-deposition.[30]

According to the Horiuti-Polanyi mechanism, the hydrogenation sequence of alkenes consists of three steps: (i) alkene adsorption on the surface of the hydrogenated metal catalyst, (ii) hydrogen migration to the *β*-carbon of the alkene with formation of a *σ*-bond between the metal and *α*-C, and finally (iii) reductive elimination of the free alkane.[71] This mechanism was adapted for the hydrogenation of dienes (*i.e.*, 1,3-cyclooctadienes (**6**)), and thus, an additional step is included (step (iv): decoordination of the monoene (*i.e.*, cyclooctene (**7**), see Scheme 4). The reaction rate of the hydrogenation of the 1,3-cyclooctadiene (**6**) was observed to be dependent on the fraction of catalyst surface covered by the substrate and zero-order with respect to hydrogen (Tables S6-S9 and Figures S10-S15). Similar effect was observed in the hydrogenation of alkenes by Ir-NPs in neat ILs.[60,61] This fact indicates that the IL in the support is present as a thin layer, which avoids mass transfer problems and increases the solubility of the hydrogen even at low pressures. Thus, the Pd-NP surfaces are always saturated with hydrogen. The non-dependence on hydrogen pressure was also observed for the surface cover for all substrate concentrations (Table S9 and Figure S15).

Scheme 4. Kinetic constants involved in the simplified mechanism for the selective hydrogenation of 1,3-cyclooctadiene by Pd-NPs.

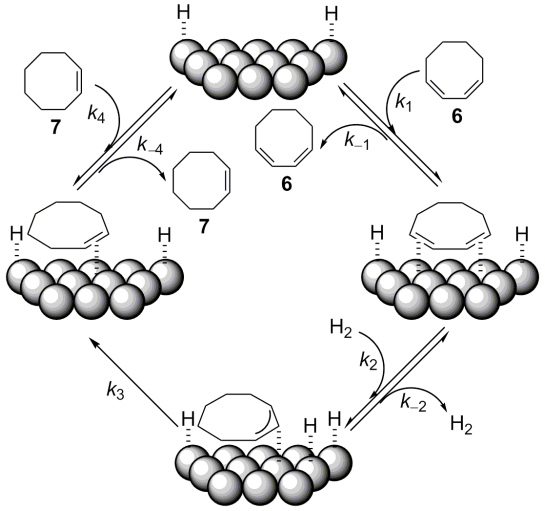

The initial rate reaction is not affected by the 1,3-cyclooctadiene (**6**) and cyclooctene (**7**) concentration, which is in agreement to the fact that the substrate adsorption and product desorption from metal active sites are not the RDS (Tables S6-S8 and Figures S10-S14). Additionally, the product is not competing for the active sites with the substrate since the selectivity for the totally hydrogenated product cyclooctane (**8**) is very low (<1%), and the comparison of the activities of our catalytic system for the hydrogenation of dienes and alkenes revealed a high preference for the hydrogenation of the

dienes *via* reversible hydrogenation to a half-hydrogenated intermediate. The RDS in the hydrogenation of the 1,3-cyclooctadiene (**6**) is very probably the reductive elimination of this half-hydrogenated intermediate to generate monoenes, which are rapidly evicted from the Pd surface and extracted by the organic phase *akin to a catalytically active membrane*. These observations suggest that the product (cyclooctene (**7**)) is more weakly adsorbed on the Pd-NPs surface than the substrate (1,3-cyclooctadiene (**6**)), and thus, $K_1[\mathbf{6}] >>> K_4[\mathbf{7}]$ (Eq. S1). Therefore, the hydrogenation of the 1,3-cyclooctadiene (**6**) at the Pd-NPs surface is likely to be the RDS with k_2 and k_3 combined into k_r as the overall surface reaction. The overall rate law can be expressed as (Eq. 1):

$$r = k_r \frac{K_1[\mathbf{6}][*]}{1 + K_1[\mathbf{6}]} \qquad \text{(Eq. 1)}$$

A plot of natural log of k_r against the inverse of different reaction temperatures allowed estimation of the apparent activation energy ($E_{a\text{-}app}$) of the hydrogenation of the 1,3-cyclooctadiene (**6**) (Figures 4 and S16 and Table S10). The observed Arrhenius plot presented a convex curve, although quite anomalously, it represents the effect of the temperature on the association of the chemical step for the product formation with the formation/adsorption of the π-allyl intermediate ($k_r = k_3K_2$). At low temperature, this reactive intermediate predominates, exhibiting normal pre-exponential factors (A). At high temperatures, however, the reactive state dissociates, affecting the slope and exhibiting a small pre-exponential factor (A). As expected, a negative enthalpy is observed for the diene adsorption (Figure S17), confirming its exothermic nature.

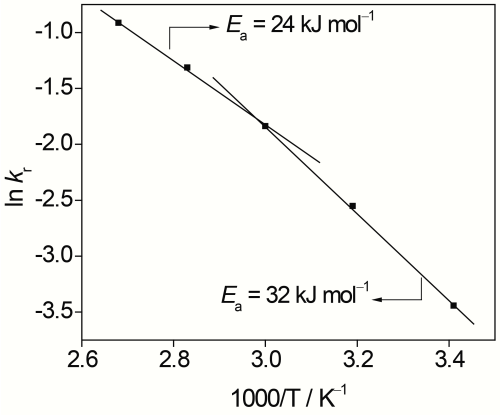

Figure 4. Arrhenius plot of the selective hydrogenation of the 1,3-cyclooctadiene by Pd/**sgPF$_6$** catalyst.

The values of E_a obtained for the reaction are determined as 24 and 32 kJ mol^{-1} and the ΔH_{app} as −14 kJ mol^{-1}. The E_a is lower than those observed for hydrogenation of non-conjugated dienes by α- and γ-alumina supported palladium catalysts (49-58 kJ mol^{-1}).[72] Finally, the selectivity is not significantly affected by changing any parameter (substrate/product concentration, hydrogen pressure and reaction temperature), which indicates again that the selectivity is inherent to the Pd-metallic surfaces in this IL-hybrid organosilica confined-like environment.

4. CONCLUSIONS

The surface area and pore diameter of IL-hybrid organosilicas based on 1-*n*-butyl-3-(3-trimethoxysilylpropyl)-imidazolium cations can be controlled by the hydrophobicity of the associated anions. The depth profile distribution of sputtered Pd-NPs on the IL-hybrid organosilica is mainly regulated by the strength of the contact ion pair formed between the imidazolium cation and the anion rather than the IL-hybrid organosilica pore size and surface area. Higher Pd-NPs concentrations are found inside the supports for systems with strong contact ion pairs. The Pd^0 surface component decreases with the increase of the ionic strength between the imidazolium cation and anions (contact ion pair). The diffusion of the sputtered metal atoms or clusters is limited by the presence of reactive species (imidazolium ionic liquids with low cation-anion strength).

The observed high activity (TOF up to 11.6 s^{-1}), productivity (TON up to 5000) and selectivity (up to ≥99%) to monoenes at full diene conversion is likely to be a result of the intrinsically electron deficient Pd-metallic surfaces and the distinct affinity/diffusion of the diene and monoenes in this IL-hybrid organosilica environment. This suggests that the catalysts under the multiphase regime ("dynamic asymmetric mixture") operate akin to *catalytically active membranes*, *i.e.* away from the thermodynamic equilibrium. Finally, the Horiuti-Polyani mechanism can be extended to this catalytic system and the rate-determining step appears to be the reductive elimination-like path involving a π-allyl intermediate and the metal-hydride species, generating the partially hydrogenated product that is rapidly evicted from the "IL-membrane" to the organic phase.

ASSOCIATED CONTENT

Supporting Information

Detailed description of the material included in the SI. This material is available free of charge via the Internet at http://pubs.acs.org.

AUTHOR INFORMATION

Corresponding Author

*Phone: +44 (0) 115 748 4613. Fax: +44 (0) 115 951 3555. E-mail: Jairton.Dupont@nottingham.ac.uk

Notes

The authors declare no competing financial interest.

ACKNOWLEDGMENT

We would like to thank CNPq, CAPES, FAPERGS, INCT-Catal., and PETROBRAS for providing financial support for this work and the LNLS staff.

REFERENCES

(1) Shi, J. *Chem. Rev.* **2013**, 113, 2139-2181.
(2) Tauster, S. J.; Fung, S. C.; Garten, R. L. *J. Am. Chem. Soc.* **1978**, 100, 170-175.
(3) Tauster, S. J. *Acc. Chem. Res.* **1987**, 20, 389-394.
(4) Stakheev, A. Y.; Kustov, L. M. *Appl. Catal., A Gen.* **1999**, 188, 3-35.
(5) Bernal, S.; Calvino, J. J.; Cauqui, M. A.; Gatica, J. M.; López Cartes, C.; Pérez Omil, J. A.; Pintado, J. M. *Catal. Today* **2003**, 77, 385-406.
(6) Trovarelli, A.; Dolcetti, G.; Deleitenburg, C.; Kaspar, J.; Finetti, P.; Santoni, A. *J. Chem. Soc. Faraday* **1992**, 88, 1311-1319.

(7) Fehér, C.; Kriván, E.; Kovács, J.; Hancsók, J.; Skoda-Földes, R. *J. Mol. Catal. A: Chem.* **2013**, 372, 51-57.
(8) Sobota, M.; Schmid, M.; Happel, M.; Amende, M.; Maier, F.; Steinruck, H. P.; Paape, N.; Wasserscheid, P.; Laurin, M.; Gottfried, J. M.; Libuda, J. *Phys. Chem. Chem. Phys.* **2010**, 12, 10610-10621.
(9) Silveira, E. T.; Umpierre, A. P.; Rossi, L. M.; Machado, G.; Morais, J.; Soares, G. V.; Baumvol, I. L. R.; Teixeira, S. R.; Fichtner, P. F. P.; Dupont, J. *Chem. Eur. J.* **2004**, 10, 3734-3740.
(10) Prost, J.; Manneville, J. B.; Bruinsma, R. *Eur. Phys. J. B* **1998**, 1, 465-480.
(11) Schoonheydt, R. A.; Weckhuysen, B. M. *Phys. Chem. Chem. Phys.* **2009**, 11, 2794-2798.
(12) Leenders, S. H.; Gramage-Doria, R.; de Bruin, B.; Reek, J. N. *Chem. Soc. Rev.* **2015**, 44, 433-448.
(13) Parmon, V. N. *Catal. Today* **1999**, 51, 435-456.
(14) Bedeaux, D.; Kjelstrup, S.; Zhu, L.; Koper, G. J. *Phys. Chem. Chem. Phys.* **2006**, 8, 5421-5427.
(15) Sheehan, D. P.; Mallin, D. J.; Garamella, J. T.; Sheehan, W. F. *Found. Phys.* **2014**, 44, 235-247.
(16) Sheehan, D. P. *Phys. Rev. E* **2013**, 88, 032125.
(17) Sievers, C.; Jimenez, O.; Müller, T. E.; Steuernagel, S.; Lercher, J. A. *J. Am. Chem. Soc.* **2006**, 128, 13990-13991.
(18) Luza, L.; Gual, A.; Rambor, C. P.; Eberhardt, D.; Teixeira, S. R.; Bernardi, F.; Baptista, D. L.; Dupont, J. *Phys. Chem. Chem. Phys.* **2014**, 16, 18088-18091.
(19) Neouze, M.; Le Bideau, J.; Leroux, F.; Vioux, A. *Chem. Commun.* **2005**, 1082-1084.
(20) Delahaye, E.; Göbel, R.; Löbbicke, R.; Guillot, R.; Sieber, C.; Taubert, A. *J. Mater. Chem.* **2012**, 22, 17140.
(21) Dai, S.; Ju, Y. H.; Gao, H. J.; Lin, J. S.; Pennycook, S. J.; Barnes, C. E. *Chem. Commun.* **2000**, 243-244.
(22) Neouze, M. A.; Kronstein, M.; Tielens, F. *Chem. Commun.* **2014**, 50, 10929-10936.
(23) Le Bideau, J.; Viau, L.; Vioux, A. *Chem Soc Rev* **2011**, 40, 907-925.
(24) Wender, H.; Migowski, P.; Feil, A. F.; Teixeira, S. R.; Dupont, J. *Coord. Chem. Rev.* **2013**, 257, 2468-2483.
(25) Gonçalves, R. V.; Migowski, P.; Wender, H.; Eberhardt, D.; Weibel, D. E.; Sonaglio, F. C.; Zapata, M. J. M.; Dupont, J.; Feil, A. F.; Teixeira, S. R. *J. Phys. Chem. C* **2012**, 116, 14022-14030.
(26) Wender, H.; de Oliveira, L. F.; Feil, A. F.; Lissner, E.; Migowski, P.; Meneghetti, M. R.; Teixeira, S. R.; Dupont, J. *Chem. Commun.* **2010**, 46, 7019.
(27) Luza, L.; Gual, A.; Dupont, J. *ChemCatChem* **2014**, 6, 702-710.
(28) W. L. F. Armarego; Perrin, D. D. *Purification of Laboratory Chemicals, Oxford (UK)*; 4th ed.; Butterworth-Heineman, 1997.
(29) Chi, Y. S.; Lee, J. K.; Lee, S.-g.; Choi, I. S. *Langmuir* **2004**, 20, 3024-3027.
(30) Luza, L.; Gual, A.; Eberhardt, D.; Teixeira, S. R.; Chiaro, S. S. X.; Dupont, J. *ChemCatChem* **2013**, 5, 2471-2478.
(31) Bussamara, R.; Eberhardt, D.; Feil, A. F.; Migowski, P.; Wender, H.; de Moraes, D. P.; Machado, G.; Papaléo, R. M.; Teixeira, S. R.; Dupont, J. *Chem. Commun.* **2013**, 49, 1273.
(32) Tolentino, H.; Compagnon-Cailhol, V.; Vicentin, F. C.; Abbate, M. *J. Synchot. Rad.* **1998**, 5, 539-541.
(33) Shafeev, G. A.; Themlin, J. M.; Bellard, L.; Marine, W.; Cros, A. *J. Vac. Sci. Technol. A* **1996**, 14, 319-326.
(34) Koningsberger, D. C.; Prins, R. *X-ray Absorption: Principles, applications and techniques of EXAFS, SEXAFS and XANES in Chemical Analysis; Chemical Analysis*; John Wiley & Sons: New York, 1988; Vol. 92.
(35) Newville, M. *J. Synchot. Rad.* **2001**, 8, 322-324.
(36) Zabinsky, S. I.; Rehr, J. J.; Ankudinov, A.; Albers, R. C.; Eller, M. J. *Phys. Rev. B* **1995**, 52, 2995-3009.
(37) El Kadib, A.; Hesemann, P.; Molvinger, K.; Brandner, J.; Biolley, C.; Gaveau, P.; Moreau, J. J. E.; Brunel, D. *J. Am. Chem. Soc.* **2009**, 131, 2882-2892.
(38) Coasne, B.; Viau, L.; Vioux, A. *J. Phys. Chem. Lett.* **2011**, 2, 1150-1154.
(39) Gozzo, F. C.; Santos, L. S.; Augusti, R.; Consorti, C. S.; Dupont, J.; Eberlin, M. N. *Chem. Eur. J.* **2004**, 10, 6187-6193.
(40) Marsavelski, A.; Smrecki, V.; Vianello, R.; Zinic, M.; Mogus-Milankovic, A.; Santic, A. *Chem. Eur. J.* **2015**, 21, 12121-12128.
(41) Delahaye, E.; Gobel, R.; Lobbicke, R.; Guillot, R.; Sieber, C.; Taubert, A. *J. Mater. Chem.* **2012**, 22, 17140-17146.
(42) Sun, J.; Li, X.; Taguchi, A.; Abe, T.; Niu, W.; Lu, P.; Yoneyama, Y.; Tsubaki, N. *ACS Catal.* **2014**, 4, 1-8.
(43) Torimoto, T.; Okazaki, K.-i.; Kiyama, T.; Hirahara, K.; Tanaka, N.; Kuwabata, S. *Appl. Phys. Lett.* **2006**, 89, 243117-243113.
(44) Wender, H.; de Oliveira, L. F.; Migowski, P.; Feil, A. F.; Lissner, E.; Prechtl, M. H. G.; Teixeira, S. R.; Dupont, J. *J. Phys. Chem. C* **2010**, 114, 11764-11768.
(45) Wender, H.; Migowski, P.; Feil, A. F.; de Oliveira, L. F.; Prechtl, M. H. G.; Leal, R.; Machado, G.; Teixeira, S. R.; Dupont, J. *Phys. Chem. Chem. Phys.* **2011**, 13, 13552-13557.
(46) Gong, X.; Frankert, S.; Wang, Y.; Li, L. *Chem Commun (Camb)* **2013**, 49, 7803-7805.
(47) Lamber, R.; Wetjen, S.; Jaeger, N. I. *Phys. Rev. B* **1995**, 51, 10968-10971.
(48) Ohba, T.; Kubo, H.; Ohshima, Y.; Makita, Y.; Nakamura, N.; Uehara, H.; Takakusagi, S.; Asakura, K. *Chem. Lett.* **2015**, 44, 803-805.
(49) Heinemann, K.; Poppa, H. *Surf. Sci.* **1985**, 156, 265-274.
(50) Goyhenex, C.; Henry, C. R.; Urban, J. *Philos. Mag. A* **1994**, 69, 1073-1084.
(51) Jacobs, J. W. M.; Schryvers, D. *J. Catal.* **1987**, 103, 436-449.
(52) Wanger, C. D.; Riggs, W. M.; Davis, L. E.; Moulder, G. E.; Mulenberg, G. E. *Handbook of X-ray Photoelectron Spectroscopy* Perkin-Elmer Corp.: Minnesota, 1979.
(53) Mason, M. G.; Gerenser, L. J.; Lee, S. T. *Phys. Rev. Lett.* **1977**, 39, 288-291.
(54) Zanatta, M.; Girard, A. L.; Simon, N. M.; Ebeling, G.; Stassen, H. K.; Livotto, P. R.; dos Santos, F. P.; Dupont, J. *Angew. Chem. Int. Ed.* **2014**, 53, 12817-12821.
(55) Stassen, H. K.; Ludwig, R.; Wulf, A.; Dupont, J. *Chem. Eur. J.* **2015**, 21, 8324-8335.
(56) Dupont, J.; Meneghetti, M. R. *Curr. Opin. Colloid Interface Sci.* **2013**, 18, 54-60.
(57) Machado, G.; Scholten, J. D.; de Vargas, T.; Teixeira, S. R.; Ronchi, L. H.; Dupont, J. *Int. J. Nanotechnol.* **2007**, 4, 541-563.
(58) Kauling, A.; Ebeling, G.; Morais, J.; Padua, A.; Grehl, T.; Brongersma, H. H.; Dupont, J. *Langmuir* **2013**, 29, 14301-14306.
(59) Van Santen, R. A. *Acc Chem Res* **2009**, 42, 57-66.
(60) Fonseca, G. S.; Domingos, J. B.; Nome, F.; Dupont, J. *J. Mol. Catal. A: Chem.* **2006**, 248, 10-16.
(61) Dupont, J.; Fonseca, G. S.; Umpierre, A. P.; Fichtner, P. F. P.; Teixeira, S. R. *J. Am. Chem. Soc.* **2002**, 124, 4228-4229.
(62) Umpierre, A. P.; de Jesús, E.; Dupont, J. *ChemCatChem* **2011**, 3, 1413-1418.
(63) Vasquez, N.; Madix, R. J. *J. Catal.* **1998**, 178, 234-252.
(64) Guo, X. C.; Madix, R. J. *J. Catal.* **1995**, 155, 336-344.

(65) Freidlin, L.; Litvin, Y. *Petr. Chem. U.S.S.R.* **1965**, 4, 111-116.
(66) Tanaka, H. *J. Phys.: Condens. Matter* **2000**, 12, R207-R264.
(67) Yi, J.; Tavlarides, L. L. *AlChE J.* **1992**, 38, 1957-1968.
(68) Whitesides, G. M.; Grzybowski, B. *Science* **2002**, 295, 2418-2421.
(69) Umpierre, A. P.; Machado, G.; Fecher, G. H.; Morais, J.; Dupont, J. *Adv. Synth. Catal.* **2005**, 347, 1404-1412.
(70) Dupont, J.; Suarez, P.; Umpierre, A.; de Souza, R. *J. Braz. Chem. Soc.* **2000**, 11, 293-297.
(71) Mattson, B.; Foster, W.; Greimann, J.; Hoette, T.; Le, N.; Mirich, A.; Wankum, S.; Cabri, A.; Reichenbacher, C.; Schwanke, E. *J. Chem. Educ.* **2013**, 90, 613-619.
(72) Fernández, M. B.; Tonetto, G. M.; Crapiste, G.; Damiani, D. E. *Int. J. Chem. React. Eng.* **2007**, 5, A10.